IEEE Access
Multidisciplinary | Rapid Review | Open Access Journal

Received May 30, 2020, accepted June 21, 2020, date of publication June 25, 2020, date of current version July 3, 2020.

Digital Object Identifier 10.1109/ACCESS.2020.3004860

Convolutional Neural Network (CNN)-Based Fast Back Projection Imaging With Noise-Resistant Capability

GUANQUN SUN AND FANGZHENG ZHANG, (Senior Member, IEEE)
Key Laboratory of Radar Imaging and Microwave Photonics, Ministry of Education, Nanjing University of Aeronautics and Astronautics, Nanjing 210016, China

Corresponding author: Fangzheng Zhang (zhangfangzheng@nuaa.edu.cn)

This work was supported in part by the National Natural Science Foundation of China under Grant 61871214, in part by the Natural Science Foundation of Jiangsu Province under Grant BK20180066, in part by the Jiangsu Provincial Program for High-Level Talents in Six Areas under Grant DZXX-005, in part by the Fundamental Research Funds for the Central Universities under Grant NS2018028, and in part by the Foundation of Graduate Innovation Center in NUAA under Grant kfjj20190401.

ABSTRACT We propose and demonstrate a convolutional neural network (CNN)-based fast back projection (FBP) imaging method, which has noise-resistant capability in strong noise conditions. In this method, the desired high-resolution image is constructed from a low-resolution back projection (BP) image using a pre-trained CNN. Compared to the high-resolution imaging with basic BP algorithm, the proposed CNN-based FBP imaging has significantly reduced complexity, enabling a fast imaging speed. Meanwhile, by training the CNN using noiseless images as the desired output, the CNN-based FBP imaging is noise-resistant, which helps to obtain high-quality images in strong noise scenarios. Performance of this CNN-based FBP imaging method is investigated and compared with basic BP imaging and other methods through extensive numerical simulations. The results show that, using a CNN with optimized structure, the proposed method can greatly improve the imaging speed. Meanwhile, high-quality images with improved peak signal to noise ratios (PSNRs) are obtained in low signal-to-noise-ratio (SNR) conditions. This CNN-based FBP imaging method is expected to find applications where high-quality and fast radar imaging is required.

INDEX TERMS Synthetic aperture radar, back projection algorithm, fast back projection imaging, convolutional neural network, high-resolution imaging.

I. INTRODUCTION

High-resolution radar imaging has wide applications in automatic driving, security checks, environmental monitoring, and so on [1], [2]. Synthetic aperture radar (SAR) imaging is a powerful technique to obtain high-resolution images taking advantage of the relative motion between radar and target [3], [4]. Among the various SAR imaging algorithms, the time-domain back projection (BP) imaging algorithm is regarded as a general imaging approach that can be adapted to arbitrary aperture geometries [5]–[8]. Besides, the BP imaging algorithm is simple to implement without complicated nonlinear motion compensation, which is usually required in frequency-domain SAR imaging algorithms [9]. The main drawback of BP imaging algorithm is that it requires a large number of computations [10], which limits the imaging speed and makes it difficult to achieve fast or real-time radar imaging. To address this problem, a number of fast back projection (FBP) imaging algorithms have been proposed, which apply sparse sampling in the along-track direction to enhance the imaging speed [11]–[13]. In these FBP imaging algorithms, the total synthetic aperture is usually split into multiple sub-apertures, and each sub-aperture generates a coarse image. Then, all the coarse images are recursively fused by image-domain interpolations to get the final image. These FBP algorithms have been proved feasible to improve the imaging speed, but the image quality may be deteriorated compared with that by using the basic BP imaging algorithm, especially when the radar suffers from strong noises. Although the influence of noise on FBP imaging has been considered in previous works [14], [15], effective solutions to improving the image quality are rarely reported. Considering that the radar usually works in low signal-to-noise-ratio (SNR) environments, it is highly demanded to find effective approaches to simultaneously increase the BP imaging speed and generate noise-resistant high-quality images.

The associate editor coordinating the review of this manuscript and approving it for publication was Hasan S. Mir.

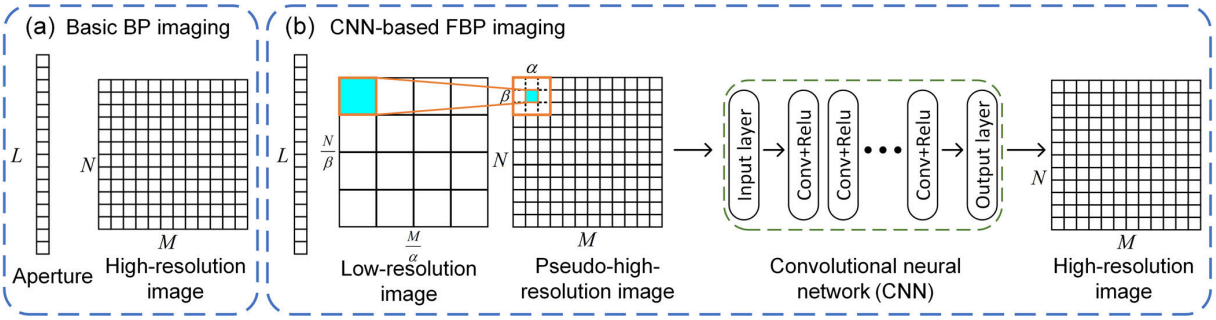

FIGURE 1. Illustrations of (a) basic BP imaging and (b) the proposed CNN-based FBP imaging.

In recent years, deep learning technology, especially the convolutional neural network (CNN) has emerged as a powerful tool for image construction and processing [16]–[18]. Previously, the CNN has been successfully applied to implement speckle elimination [19], [20], target classification [21], [22], and recognition [23] in the field of SAR imaging. Besides, CNN-based fast computed tomography (CT) image construction has also been proposed to address the sparse-view problem [24]. In this paper, we propose and demonstrate a CNN-based FBP radar imaging method, which is noise-resistant when the radar is operated in low SNR conditions. In this method, the desired high-resolution image is constructed from a low-resolution BP image through a pre-trained CNN. Compared with the basic BP imaging algorithm, the CNN-based FBP imaging method has significantly reduced complexity, which ensures a fast imaging speed. In addition, the CNN is trained considering different radar imaging scenes to establish a mapping between low-resolution BP images and noiseless high-resolution BP images. This way, the obtained high-resolution images by the CNN-based FBP method have a good quality with less noise interference, especially when the radar works in strong noise conditions. Performance of the proposed CNN-based FBP imaging method is investigated through simulations. Its imaging speed and quality are compared with basic BP imaging and other methods.

II. PRINCIPLE

Fig. 1(a) is a schematic illustration of the basic BP imaging method, in which the radar aperture moves along a linear track to form a synthetic aperture with L equally spaced apertures. For each aperture, pulse compression is first implemented to obtain the 1D pulse compression image. After interpolating the 1D pulse compression image to make it coincide with the $M \times N$ pixels of the imaging area, the 1D coarse image of the l-th aperture ($l = 1, 2, \ldots, L$) is obtained, as denoted by R_l (t_{ij}), where t_{ij} is the round-trip time delay between the l-th aperture and the image pixel at the coordinate of (x_i, y_j). Then, the coarse images of all the apertures are coherently accumulated to get the amplitude of the image pixel at (x_i, y_j), which is expressed as

$$A(x_i, y_i) = \sum_{m=1}^{L} R_m(t_{ij}) \exp\left(j\frac{4\pi t_{ij} c}{2\lambda}\right) \tag{1}$$

where c is the speed of light and λ is the carrier wavelength. By calculating the amplitudes at different pixels, the final image can be obtained. In the basic BP algorithm, the number of required operations is proportional to $L \times M \times N$. It is usually time-consuming to construct a high-resolution image because of the high computational complexity. To address this, we propose the CNN-based FBP imaging method that uses a pre-trained CNN to construct the desired high-resolution images from low-resolution BP images.

Fig. 1(b) shows the principle of the CNN-based FBP imaging method. Assuming the desired high-resolution image contains $M \times N$ pixels, a low-resolution image with $(M/\alpha) \times (N/\beta)$ pixels (α, β, M/α, and N/β are positive integers) is first generated by the basic BP imaging method. Based on this low-resolution image, a pseudo-high-resolution image with $M \times N$ pixels covering the same imaging area is derived as the input of the CNN. The pseudo-high-resolution image is divided into $(M/\alpha) \times (N/\beta)$ blocks with each block containing $\alpha \times \beta$ sub-pixels. The detailed approach for getting the pseudo-high-resolution image is as follows. A random sub-pixel in a given block is assigned with the same value as the low-resolution image pixel corresponding to this block, as shown in Fig. 1(b). The other sub-pixels in this block are simply set to zero. Before the previous processing, all the pixels are normalized to the range between 0 and 1 for each image. The obtained pseudo-high-resolution image is sent to the pre-trained CNN that outputs the desired high-resolution image. The CNN consists of one input layer, multiple middle layers, and one output layer. The input layer operates on the pseudo-high-resolution image. Each middle layer contains a convolution layer and a rectified linear unit (ReLU) as the nonlinear activation function [19]. The output layer is composed of a convolution layer and a regression layer. Here, the regression layer predicts the responses of the trained network and thus helps to stabilize the training for regression [25]. All the convolution layers in the CNN have the same number of filters and the same filter size. Zero-padding is adopted to make sure the pixels at the image boundary can be correctly predicted. The dataset used for training the CNN is numerically generated. To make sure the CNN-based FBP imaging method is applicable in different scenarios, the pseudo-high-resolution images are generated considering different conditions in which the number of targets, the target

locations, and SNR of the radar echoes are randomly chosen within a specific range. The ground truth images used for training the CNN is the high-resolution images obtained by basic BP method without noise. When training the CNN, the mean square error (MSE) between the output image and the ground truth image is used as the loss function:

$$Loss(\Theta) = \frac{1}{MN}\sum_{i}^{M}\sum_{j}^{N}\left\| Y_{i,j}^{\Theta} - X_{i,j}^{ground} \right\|_2^2 \qquad (2)$$

where $Y_{i,j}^{\Theta}$ and $X_{i,j}^{ground}$ denote the i,j-th pixel of the network's output image and the corresponding ground truth, respectively. The output image Y^{Θ} is given by $Y^{\Theta} = F\left(X^{input};\Theta\right)$, where F is the CNN's operator on the input image X^{input} and Θ is the CNN's parameter space (e.g., kernels, weights, and biases). To suppress the gradients explosion due to a small learning rate and improve the training speed as much as possible, adjustable gradient clipping is adopted in the training process. Once the CNN is trained, it can be used to generate high-resolution images by feeding new test data into the network.

In the proposed method, a simple structure of the CNN is preferred such that most of the computations of the CNN-based FBP imaging are used to construct the low-resolution BP image. Because the complexity of constructing the low-resolution BP image is reduced by a factor of $\alpha\beta$ compared to that required to construct a high-resolution BP image, a significantly improved imaging speed can be achieved by the CNN-based FBP imaging method. To further enhance the imaging speed, the CNN-based FBP method can be applied together with other FBP algorithms, i.e., the imaging speed of the CNN-based FBP method can be further increased if the low-resolution image is generated by an existed FBP method. In addition to the improvement of imaging speed, another advantage of the proposed method is that it is noise-resistant, because the CNN is trained using noiseless images as the desired outputs. This property makes it feasible to get high-quality images, especially in strong noise scenarios.

III. SIMULATION AND RESULTS

To investigate the performance of the proposed CNN-based FBP method, a large number of numerical simulations are carried out. In the simulation, the radar transmits linearly frequency modulated signals with a bandwidth of 4 GHz. The conceptual picture of the simulation scenario is shown in Fig. 2, where the linear synthetic aperture is composed of 100 apertures ($L = 100$) with a total length of 2.5 m. The imaging area is 50 m away from the radar and has a size of 2 m $\times$ 2 m. The desired high-resolution image has 256 $\times$ 256 pixels, and the low-resolution BP image used for generating the pseudo-high-resolution image has 64 $\times$ 64 pixels. The target is a series of point reflectors, of which the total number is randomly chosen from 1 to 300 and the positions are randomly assigned within the imaging area. When generating a pseudo-high-resolution image,

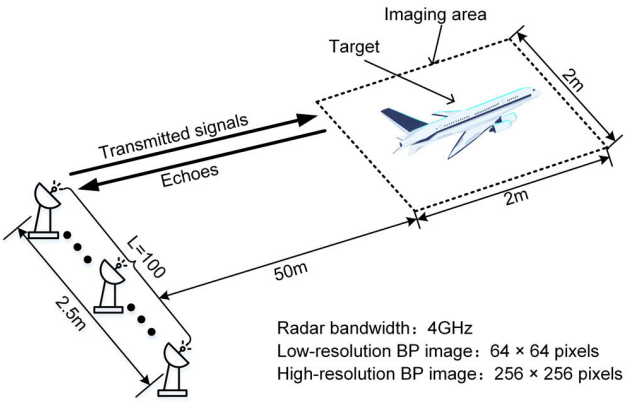

FIGURE 2. The conceptual picture of the simulation scenario.

additive white Gaussian noise (AWGN) is loaded to the radar echo, imitating a radar receiver with a random SNR between -35 dB and -5 dB. The corresponding ground truth images are generated by basic BP imaging algorithm without considering the noise. The dataset used for training and validating the CNN is composed of 10,000 high-resolution images and the corresponding ground truth images, of which 80% is used as the training set and the other 20% is the validation set. Because the performance and running speed of the CNN is closely related to its structure, especially the middle layers, the network parameters including the number of middle layers, and the filter number and size in each convolution layer are optimized to achieve a tradeoff between fast imaging speed and high imaging quality. The optimized CNN has 4 middle layers and each convolution layer has 16 filters with a size of 3 $\times$ 3. The CNN is trained using the Stochastic Gradient Descent Momentum (SGDM) optimization [25]. The learning rate is initially set to 0.2, and it is decreased by a factor of 10 for every 10 epochs. Meanwhile, gradient clipping is enabled using L2-norm of the gradients, in which the threshold is set to 0.01. The CNN is trained by a computer (denoted by Comp. 1) with its specifications listed in Table 1. The loss curves for training the CNN are shown in Fig. 3, in which both the training loss and the validation loss are well converged after 100 epochs of training.

TABLE 1. Specifications of the computers and imaging time comparison.

	CPU (Intel)	RAM	GPU	Time (Basic BP)	Time (CNN-FBP)
Comp. 1	i9-9900K (16-core)	DDR4 32 GB	RTX 2080Ti	1.5974 s	0.1043 s
Comp. 2	i5-8250U (8-core)	DDR3 8 GB	-	2.4075 s	0.1814 s

First of all, to show the performance of the CNN-based FBP method, imaging of a target with 68 point reflectors that compose a plane profile is demonstrated. Fig. 4(a) shows the low-resolution basic BP image with 64 $\times$ 64 pixels when the SNR of the radar echo is -15 dB. Based on this low-resolution image, a pseudo-high-resolution image is derived, as shown in Fig. 4(b). Using this pseudo-high-resolution image as the input of the trained CNNs, high-resolution

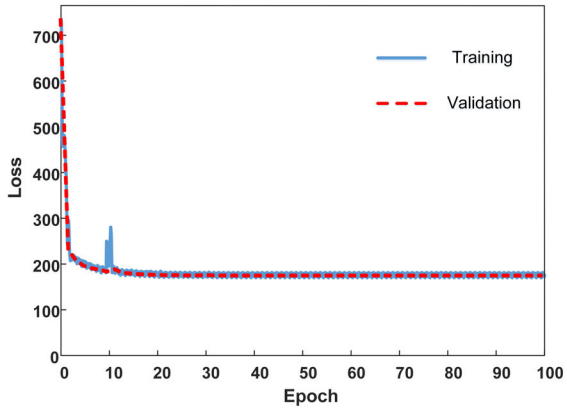

FIGURE 3. The loss performance of the CNN during training.

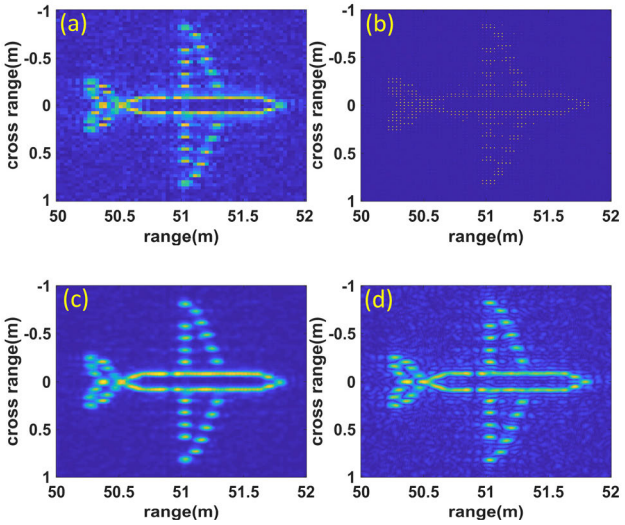

FIGURE 4. (a) The low-resolution basic BP image, (b) the pseudo-high-resolution image, (c) the CNN-based FBP image, and (d) the high-resolution BP image when the SNR is −15 dB.

images with 256 × 256 pixels are obtained. Fig. 4(c) is the image constructed by the CNN-based FBP method. The resolution of the image in Fig. 4(c) is obviously improved compared with that of the image in Fig. 4(a), verifying the capability of the proposed method for constructing high-resolution images from low-resolution images. As a comparison, the high-resolution basic BP image is shown in Fig. 4(d). It is found that, the CNN-based FBP image in Fig. 4(c) has a slightly cleaner background, compared with the image in Fig. 4(d). This result is attributed to the noise-resistant property of the CNN-based FBP imaging method.

In the previous demonstration, the computations required for constructing the low-resolution BP image is one-sixteenth ($\alpha\beta = 16$) of that required for generating the high-resolution basic BP image. Therefore, the CNN-based FBP imaging method can enhance the imaging speed by a factor close to 16. To check this property, we compare the time used to generate the image in Fig. 4(c) with that required to obtain the image in Fig. 4(d). First, we use the same computer (Comp. 1) as the one used for training the CNN to measure the imaging time. As shown in Table 1, the time required for basic BP imaging and CNN-based FBP imaging is 1.5947 s, and 0.1043 s, respectively. Thus, the CNN-based FBP reduces the imaging time by a factor of ∼15.3, which is close to the expectation. We also test the imaging time using a laptop with a lower computation speed that is comparative with the commonly used commercial computers. Specifications of the adopted laptop are also listed in Table 1 (denoted by Comp. 2). In this case, the time used for high-resolution basic BP imaging and CNN-based FBP imaging is 2.4075 s and 0.1814 s, respectively, with a reduction ratio of ∼13.3. Therefore, with common computer facilities, the CNN-based FBP method can still significantly enhance the imaging speed.

To quantitatively evaluate the imaging quality, peak signal to noise ratios (PSNRs) [26] of the high-resolution images obtained by basic BP method and CNN-based FBP method are calculated when the radar works in different SNRs. In the simulation, the target number and distribution are the same as those used in obtaining Fig. 4. The noise-free high-resolution BP image, as shown in Fig. 5(a), is used as the reference to calculate the PSNR:

$$PSNR = 10\log_{10}\left(\frac{1}{MSE}\right) = 10\log_{10}\left(\frac{MN}{\sum_{i}^{M}\sum_{j}^{N}\left\|X_{i,j}^{test} - X_{i,j}^{ref}\right\|_2^2}\right) \quad (3)$$

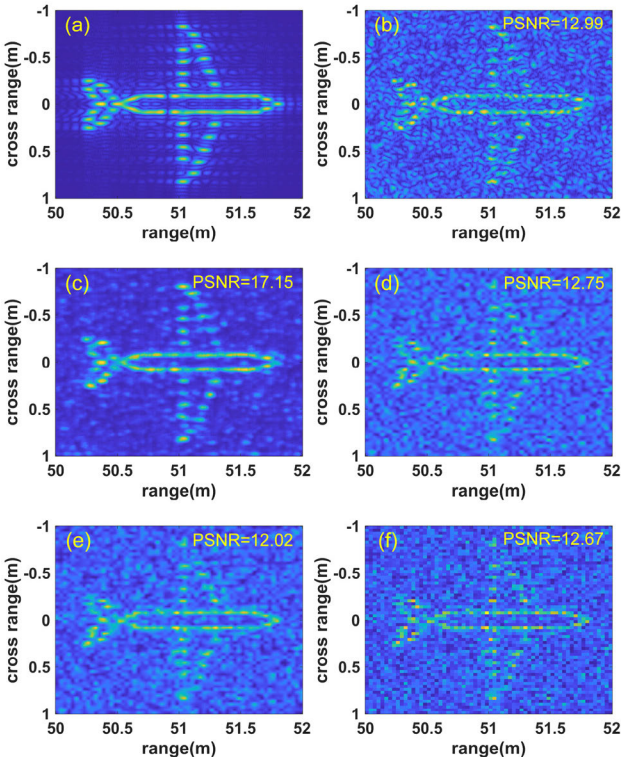

FIGURE 5. (a) The noiseless reference high-resolution BP image, and the images obtained by (b) high-resolution basic BP imaging, (c) CNN-based FBP imaging, (d) bicubic interpolation, (e) bilinear interpolation, and (f) nearest interpolation when the SNR is −35 dB.

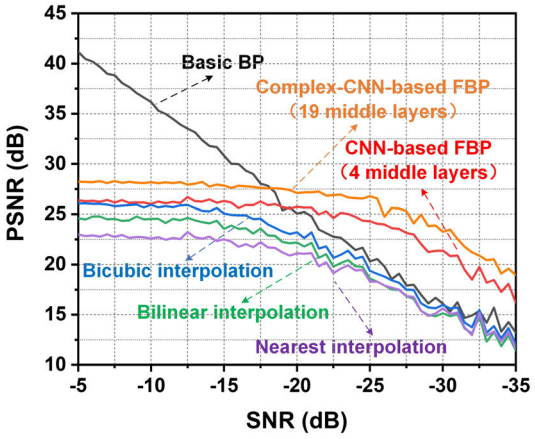

FIGURE 6. PSNR of the high-resolution images obtained by different methods when the SNR decreases from −5 dB to −35 dB.

in which X^{test} and X^{ref} are the image under test and the reference image, respectively. Fig. 6 shows the measured PSNR as the SNR decreases from −5 dB to −35 dB with a step of 0.5 dB. In Fig. 6, the CNN-based FBP imaging achieves higher PSNR when the SNR is lower than −18 dB, while, the basic BP imaging performs better when the SNR is higher than −18 dB. The results indicate that the CNN-based FBP imaging has better performance in strong-noise condition, which is attributed to its noise-resistant property. Besides, as the SNR decreases, the noise-resistant capability of the CNN-based FBP method is found to become more prominent. To clearly show this property, the high-resolution basic BP image and the CNN-based FBP image are shown in Fig. 5(b) and (c), respectively, when the SNR is −35 dB. It is obvious that the CNN-based FBP image has better quality with less noise interference (the PSNR is improved by over 4 dB). However, in low-noise conditions, the basic BP imaging method achieves better quality than the CNN-based FBP imaging method. This is caused by the fact that the CNN has a relatively simple structure, which achieves improved imaging speed at the expense of not ideally approaching the noiseless ground truth image. If a CNN having more complex structure is adopted, the imaging quality is expected to be improved, but the imaging speeding will be lowered because of the increased computational complexity. To show this, the PSNRs of high-resolution images constructed by a pre-trained complex CNN, which has 19 middle layers and each convolution layer has 64 filters with a size of 3×3, is provided in Fig. 6, as denoted by complex-CNN-based FBP imaging. As can be seen, the image qualities are improved by complicating the network. While, the imaging time using the laptop (comp. 2) for calculation is increased to 1.5 s, which indicates that the imaging speed is greatly reduced compared with that by using the optimized CNN-based FBP imaging. In practical applications, since the radar is usually operated in low SNR conditions, the proposed method is meaningful to get high-quality images at a very fast speed. Even in high SNR conditions, the optimized CNN can still generate images with acceptable qualities, which can be proved through the imaging results in Figs. 4(c) and (d).

Since the CNN-based high-resolution image construction from a low-resolution BP image has the same function as interpolation-based image construction, it is necessary to compare the qualities of the CNN-based FBP image and the images generated by traditional interpolation techniques. To do this, the low-resolution BP image with 64×64 pixels is interpolated to high-resolution images with 256×256 pixels using nearest interpolation, bilinear interpolation, and bicubic interpolation, respectively. The PSNRs of the obtained images under different SNRs are also plotted in Fig. 6. When the SNR is higher than −25 dB, the image obtained by bicubic interpolation has a higher PSNR than those generated by the other two interpolation techniques. When the SNR is lower than −25 dB, the PSNRs are significantly reduced due to serious noise effect, and the three interpolation methods have similar performance. It is also obvious that, the CNN-based FBP imaging method performs better than all the interpolation-based methods, especially in strong-noise conditions, i.e., the advantage of the CNN-based FBP method is more obvious when the SNR is lower than −15 dB. Figs. 5(d), (e) and (f) show the high-resolution images obtained by the three interpolation techniques when the SNR is −35 dB. Compared with these images, the CNN-based FBP image has better quality (the PSNR is higher by about 5 dB), in which the target is clear and the background suffers from less noise. The result can also verify the noise-resistant capability of the CNN-based FBP imaging method.

IV. DISCUSSION

Traditional FBP imaging algorithms adopt sparse sampling in along-track direction, which mainly reduces the imaging complexity in azimuth direction. While, the proposed CNN-based FBP method reduces the imaging complexity in both range and azimuth directions. Therefore, it is capable to achieve a faster imaging speed than traditional FBP methods. To check this property, we use the FBP algorithm demonstrated in [12] to perform imaging of the same target as used in Fig. 4. When the total synthetic aperture is divided into ten sub-apertures, the FBP imaging using comp. 2 takes 1.5947 s, indicating its imaging speeding is much slower than the CNN-based FBP imaging. In addition to the advantage on imaging speed, the noise-resistant capability of the CNN-based FBP imaging method makes it more advantageous over traditional FBP methods.

In our investigation, the CNN is trained using numerically generated input and ground truth images, in which a simple AWGN model is adopted to get the radar images defected by noise. In practical applications, the radar images may be deteriorated by other undesired interference such as spurs. Thus, a comprehensive model considering these defects is preferred to generate images that are more close to real radar images. This is helpful to achieve a good performance for the trained CNN to be used in practical radar imaging scenarios. On the other hand, the CNN in the proposed method can also

be trained using real radar images. Considering that noiseless radar images are hard to obtain in practical applications, radar images collected in low-noise conditions can be used as the ground truth images.

V. CONCLUSION

We have proposed and demonstrated a CNN-based FBP imaging method aiming to increase the imaging speed and get high-quality images with suppressed noise interference. This method constructs high-resolution images from low-resolution BP images using a pre-trained CNN. Performance of the proposed method is investigated through numerical simulations with the results confirming its feasibility and advantage. We believe this CNN-based FBP imaging is a promising technique to meet the requirements where fast and high-quality radar imaging is needed.

REFERENCES

[1] J. Dickmann, N. Appenrodt, H.-L. Bloecher, C. Brenk, T. Hackbarth, M. Hahn, J. Klappstein, M. Muntzinger, and A. Sailer, "Radar contribution to highly automated driving," in *Proc. 11th Eur. Radar Conf.*, Oct. 2014, pp. 412–415.

[2] S. Stanko, D. Notel, A. Wahlen, J. Huck, F. Kloppel, R. Sommer, M. Hagelen, and H. Essen, "Active and passive mm-wave imaging for concealed weapon detection and surveillance," in *Proc. 33rd Int. Conf. Infr., Millim. THz Waves*, Sep. 2008, pp. 1–2.

[3] M. Skolnik, "An introduction and overview of radar," in *Radar Handbook*, 3rd ed. New York, NY, USA: McGraw-Hill,2008, pp. 1–24.

[4] F. Zhang, Q. Guo, Z. Wang, P. Zhou, G. Zhang, J. Sun, and S. Pan, "Photonics-based broadband radar for high-resolution and real-time inverse synthetic aperture imaging," *Opt. Express*, vol. 25, no. 14, pp. 16274–16281, Jul. 2017.

[5] G. Sun, F. Zhang, and S. Pan, "Photonic-assisted high-resolution incoherent back projection synthetic aperture radar imaging," *Opt. Commun.*, vol. 466, Jul. 2020, Art. no. 125633.

[6] D. C. Munson, J. D. O'Brien, and W. K. Jenkins, "A tomographic formulation of spotlight-mode synthetic aperture radar," *Proc. IEEE*, vol. 71, no. 8, pp. 917–925, Aug. 1983.

[7] C. Jakowatz, D. Wahl, and D. Yocky, "Beamforming as a foundation for spotlight-mode SAR image formation by backprojection," in *Proc. SPIE-Algorithms Synth. Aperture Radar Imag.*, vol. 6970, Mar. 2008, Art. no. 69700Q.

[8] S. Ozsoy and A. A. Ergin, "Pencil back-projection method for SAR imaging," *IEEE Trans. Image Process.*, vol. 18, no. 3, pp. 573–581, Mar. 2009.

[9] J. Liu, X. Qiu, L. Huang, and C. Ding, "Curved-path SAR geolocation error analysis based on BP algorithm," *IEEE Access*, vol. 7, pp. 20337–20345, 2019.

[10] L. M. H. Ulander, H. Hellsten, and G. Stenstrom, "Synthetic-aperture radar processing using fast factorized back-projection," *IEEE Trans. Aerosp. Electron. Syst.*, vol. 39, no. 3, pp. 760–776, Jul. 2003.

[11] A. F. Yegulalp, "Fast backprojection algorithm for synthetic aperture radar," in *Proc. IEEE Radar Conference. Radar Into Next Millennium*, 1999, pp. 60–65.

[12] S. Basu and Y. Bresler, "$O(N^2\log_2 N)$ filtered backprojection reconstruction algorithm for tomography," *IEEE Trans. Image Process.*, vol. 9, no. 10, pp. 1760–1773, 2000.

[13] J. Wu, Y. Li, W. Pu, Z. Li, and J. Yang, "An effective autofocus method for fast factorized back-projection," *IEEE Trans. Geosci. Remote Sens.*, vol. 57, no. 8, pp. 6145–6154, Aug. 2019.

[14] Y. Feng Shao, R. Wang, Y. Kai Deng, Y. Liu, R. Chen, G. Liu, and O. Loffeld, "Fast backprojection algorithm for bistatic SAR imaging," *IEEE Geosci. Remote Sens. Lett.*, vol. 10, no. 5, pp. 1080–1084, Sep. 2013.

[15] L. Ran, Z. Liu, T. Li, R. Xie, and L. Zhang, "An adaptive fast factorized back-projection algorithm with integrated target detection technique for high-resolution and high-squint spotlight SAR imagery," *IEEE J. Sel. Topics Appl. Earth Observ. Remote Sens.*, vol. 11, no. 1, pp. 171–183, Jan. 2018.

[16] J. Zhang, Z. Lu, M. Li, and H. Wu, "GAN-based image augmentation for finger-vein biometric recognition," *IEEE Access*, vol. 7, pp. 183118–183132, 2019.

[17] M. K. Elbashir, M. Ezz, M. Mohammed, and S. S. Saloum, "Lightweight convolutional neural network for breast cancer classification using RNA-seq gene expression data," *IEEE Access*, vol. 7, pp. 185338–185348, 2019.

[18] S. U. Rehman, S. Tu, Y. Huang, and O. U. Rehman, "A benchmark dataset and learning high-level semantic embeddings of multimedia for cross-media retrieval," *IEEE Access*, vol. 6, pp. 67176–67188, 2018.

[19] P. Wang, H. Zhang, and V. M. Patel, "SAR image despeckling using a convolutional neural network," *IEEE Signal Process. Lett.*, vol. 24, no. 12, pp. 1763–1767, Dec. 2017.

[20] S. Vitale, G. Ferraioli, and V. Pascazio, "A new ratio image based CNN algorithm for SAR despeckling," in *Proc. IEEE Int. Geosci. Remote Sens. Symp.*, Jul. 2019, pp. 9494–9497.

[21] Y. Dong, C. Wang, H. Zhang, Y. Wang, and B. Zhang, "Impact analysis of incident angle factor on high-resolution SAR image ship classification based on deep learning," in *Proc. IEEE Int. Geosci. Remote Sens. Symp.*, Jul. 2019, pp. 1358–1361.

[22] H. Zhu, W. Wang, and R. Leung, "SAR target classification based on radar image luminance analysis by deep learning," *IEEE Sensors Lett.*, vol. 4, no. 3, Mar. 2020, Art. no. 7000804.

[23] J. Lv and Y. Liu, "Data augmentation based on attributed scattering centers to train robust CNN for SAR ATR," *IEEE Access*, vol. 7, pp. 25459–25473, 2019.

[24] D. H. Ye, G. T. Buzzard, M. Ruby, and C. A. Bouman, "Deep back projection for sparse-view CT reconstruction," in *Proc. IEEE Global Conf. Signal Inf. Process. (GlobalSIP)*, Nov. 2018, pp. 1–5.

[25] J. Kim, J. K. Lee, and K. M. Lee, "Accurate image super-resolution using very deep convolutional networks," in *Proc. IEEE Conf. Comput. Vis. Pattern Recognit. (CVPR)*, Jun. 2016, pp. 1646–1654.

[26] S. Winkler and P. Mohandas, "The evolution of video quality measurement: From PSNR to hybrid metrics," *IEEE Trans. Broadcast.*, vol. 54, no. 3, pp. 660–668, Sep. 2008.

GUANQUN SUN received the B.S. degree from Northwestern Polytechnical University, Xi'an, China, in 2018. He is currently pursuing the master's degree with the Key Laboratory of Radar Imaging and Microwave Photonics, Ministry of Education, Nanjing University of Aeronautics and Astronautics.

His main research interests include photonics-based radars for high resolution imaging.

FANGZHENG ZHANG (Senior Member, IEEE) received the B.S. degree from the Huazhong University of Science and Technology, Wuhan, China, in 2008, and the Ph.D. degree from the Beijing University of Posts and Telecommunications, Beijing, China, in 2013.

He is currently a Professor with the College of Electronic and Information Engineering, Nanjing University of Aeronautics and Astronautics, and the Key Laboratory of Radar Imaging and Microwave Photonics, Ministry of Education. His current research interests include microwave photonics, radar imaging, and machine learning.